# Role of bile acid receptor FXR in development and function of brown adipose tissue

J. Yang, H.D. de Vries, Alicia Mayeuf-Louchart, J.H. Stroeve, V.W. Bloks, M. Koehorst, H. Duez, B. Staels, F. Kuipers, T. van Zutphen

# Role of bile acid receptor FXR in development and function of brown adipose tissue

J. Yang [a], H.D. de Vries [b,c], A. Mayeuf-Louchart [d], J.H. Stroeve [a,1], V.W. Bloks [a], M. Koehorst [b], H. Duez [d], B. Staels [d], F. Kuipers [a,e,*], T. van Zutphen [a,c,*]

[a] Department of Pediatrics, University of Groningen, University Medical Center Groningen, Groningen 9700RB, the Netherlands
[b] Department of Laboratory Medicine, University of Groningen, University Medical Center Groningen, Groningen 9700RB, the Netherlands
[c] Faculty Campus Fryslân, University of Groningen, Leeuwarden, the Netherlands
[d] Univ. Lille, INSERM, CHU Lille, Institut Pasteur de Lille, U1011-EGID, F-59000 Lille, France
[e] European Research Institute for the Biology of Ageing (ERIBA), University of Groningen, University Medical Center Groningen, Groningen, the Netherlands

ARTICLE INFO

*Keywords:*
Brown adipose tissue
FXR
Extracellular matrix
Cold exposure
β3-Adrenergic receptor agonist
Bile acids

ABSTRACT

Bile acids act as signalling molecules that contribute to maintenance of energy homeostasis in mice and humans. Activation of G-protein-coupled bile acid receptor TGR5 induces energy expenditure in brown adipose tissue (BAT). However, a role for the nuclear bile acid receptor Farnesoid X receptor (FXR) in BAT has remained ambiguous. We aimed to study the potential role of FXR in BAT development and functioning.

Here we demonstrate low yet detectable expression of the α1/2 isoforms of FXR in murine BAT that markedly decreases upon cold exposure. Moderate adipose tissue-specific FXR overexpression in mice induces pronounced BAT whitening, presenting with large intracellular lipid droplets and extracellular collagen deposition. Expression of thermogenic marker genes including the target of Tgr5, *Dio2*, was significantly lower in BAT of chow-fed aP2-hFXR mice compared to wild-type controls. Transcriptomic analysis revealed marked up-regulation of extracellular matrix formation and down-regulation of mitochondrial functions in BAT from aP2-hFXR mice. In addition, markers of cell type lineages deriving from the dermomyotome, such as myocytes, as well as markers of cellular senescence were strongly induced. The response to cold and β3-adrenergic receptor agonism was blunted in these mice, yet resolved BAT whitening. Newborn cholestatic Cyp2c70$^{-/-}$ mice with a human-like bile acid profile also showed distinct BAT whitening and upregulation of myocyte-specific genes, while thermogenic markers were down-regulated. *Ucp1* expression inversely correlated with plasma bile acid levels. Therefore, bile acid signalling via FXR has a role in BAT function already early in tissue development. Functionally, FXR activation appears to oppose TGR5-mediated thermogenesis.

## 1. Introduction

Bile acids exert hormone-like functions in various tissues and organs through activation of nuclear and membrane-bound receptors, such as the Farnesoid X receptor (FXR, NR1H4) and Takeda G protein-coupled receptor 5 (TGR5/GPBAR1) [1–4]. FXR is a member of the nuclear receptor superfamily that is activated particularly by relatively hydrophobic bile acids [2]. In the past years, several FXR agonists have been under development for the treatment of cholestatic liver diseases and non-alcoholic fatty liver disease (NAFLD), based on the regulatory roles of FXR in bile acid and lipid metabolism, respectively [5]. The FXR agonist obeticholic acid, which has a 100-fold greater FXR-activating potency than the natural ligand chenodeoxycholic acid (CDCA), has been FDA-approved for treatment of primary biliary cholangitis and several other agonists are in clinical development [5]. However, in addition to liver and intestine, FXR is expressed in kidney, adrenal glands, vascular wall and also in adipose tissues [6]. A number of studies have indicated a role of FXR in adipose tissue biology [7–9]. Cariou et al. found that whole-body FXR-deficient mice exhibit smaller adipocytes in white fat depots than the corresponding wild-type mice [7]. Follow-up

* Corresponding authors at: Kindergeneeskunder, University Medical Center Groningen, postbus 30.001, 9700 RB Groningen, Hanzeplein 1, 9713 GZ Groningen, the Netherlands.
*E-mail addresses:* f.kuipers@umcg.nl (F. Kuipers), t.van.zutphen@umcg.nl (T. van Zutphen).
[1] Present address: Food & Biobased Research, Bornse Weilanden 9, 6708 WG Wageningen, the Netherlands.

studies showed that FXR-deficiency reduces fat mass and insulin resistance in mouse models of genetic and diet-induced obesity [10]. Abdelkarim et al. showed that FXR has a role in white adipocyte differentiation and function via the peroxisome proliferator-activated receptor-γ (PPARγ) and Wnt/β-catenin pathways [11]. Moreover, we have recently reported that moderate overexpression of human FXR in murine adipose tissues gives rise to a reduced number of enlarged adipocytes in various WAT depots that were unable to accommodate fat storage during dietary caloric overload [12]. Taken together, these results identified a role for FXR in white adipose tissue (WAT) function. Although in earlier reports expression of *Fxr* was not detected in adult murine brown adipose tissue (BAT), whole body FXR-deficient mice were found to be cold-intolerant [13,14], indicating a potential role of FXR also in BAT.

In humans, BAT was considered to be mainly present and functional in newborns [15]. However, application of positron emission tomography (PET) and computed tomography (CT) imaging enabled the identification of active BAT also in adults [16–18]. In addition to its thermogenic effects, activated BAT has a large capacity for glucose and lipid uptake [19–21]. A recent study, based on 18F-FDG PET/CT scans from 52,487 patients, indicated a role for BAT in cardiometabolic health [22]. Hence, BAT is currently considered an attractive therapeutic target for the treatment of features of the metabolic syndrome [23].

Apart from activation of classical BAT, 'browning' of WAT is considered an important metabolic adaptation [24]. These so-called brite/beige adipocytes located in various WAT depots can contribute to thermogenesis. Several pharmacological and nutraceutical interventions have been evaluated for their potency to induce browning of WAT [21,25–27]. For instance, fexaramine, a gut-restricted FXR agonist, has been shown to promote WAT browning and to increase energy utilization by BAT without entering the bloodstream. This effect was ascribed to enhanced formation of the secondary bile acid lithocholic acid (LCA), a known FXR and TGR5 agonist [28]. Watanabe et al. reported that activation of TGR5 induces energy expenditure in BAT of high fat diet-fed mice and prevents body weight gain by the induction of the cyclic-AMP-dependent thyroid hormone activating enzyme type 2 iodothyronine deiodinase (*Dio2*) [13]. It has also been reported that long-term treatment with an FXR agonist results in a reduction in markers of BAT function, which was ascribed to a reduction in bile acid pool size and consequently lower plasma bile acid concentrations [29]. Yet, a potential, direct role of FXR in BAT development and function has not been established thus far. Therefore, we employed a mouse model of moderate overexpression of the human FXR isoform α2 in adipose tissues under the control of the aP2 (*Fabp4*) promoter [12] to evaluate the role of FXR in murine BAT. In addition, recently generated Cyp2c70-deficient mice with a human-like bile acid profile lacking FXR antagonistic muricholates that show features of neonatal cholestasis [30,31], were employed to directly assess the role of high plasma bile acid levels on BAT features in early life. Our data demonstrate that bile acid signalling via FXR has a role in BAT development and functionally opposes TGR5-mediated thermogenesis.

## 2. Materials and methods

### 2.1. Mice

Adipocyte-specific human-FXR transgenic mice (aP2-hFXR mice) were generated by microinjection of the construct into fertilized FVB/NHsd eggs. Transgene construction was described in detail by van Zutphen et al. [12]. Mice were backcrossed to C57BL6/J for five generations. Wild-type littermates were used as a control. Eight-week old male aP2-hFXR mice and control mice were housed individually in a light (12:12)-controlled and temperature (21 °C)-controlled facility and received laboratory chow and water ad libitum. Body weights were recorded weekly. At 12-week of age, animals were fasted for 4 h and then terminated under anaesthesia. Blood was collected and organs and tissues were carefully dissected, weighed and stored at −80 °C before use.

For GW4064 studies, a cohort of mice aged 13 to 16 weeks were administered GW4064 (30 mg/kg) (Sigma-Aldrich G5172, Saint Louis, MO, USA) or vehicle (sunflower oil) by daily oral gavage for one week. Mice were also fed with high-fat diet (60 % kcal from fat, D12492, ResearchDiets, New Brunswick, USA) during this week. The last gavage was given to mice 4 h before the termination. Organs and tissues were dissected and stored at −80 °C before use.

For microarray analysis BAT was collected after a 4 h fast from 10-week old male aP2-hFXR mice and control mice fed regular chow diet.

For cold exposure studies, a cohort of 12-week old wild type and a cohort of 14-week old male aP2-hFXR mice and age-matched control littermates were exposed to 4 °C (cage temperature was gradually reduced from 21 °C to 4 °C within 4 h). Locomoter activity was recorded throughout the duration of the experiment.

For β3-adrenergic receptor agonist studies, cohorts of male aP2-hFXR mice and age-matched control littermates aged 16 to 20 weeks were subcutaneously injected with CL316243 (1 mg/kg; Tocris, Bristol United Kingdom) for seven consecutive days. At the day of organ harvest, the mice were injected with the CL316243 and subsequently fasted for 4 h before necropsy.

Cyp2c70-deficient ($Cyp2c70^{-/-}$) mice were generated using CRISPR/Cas9-technology [30]. Offspring was housed with their dam on chow diet (Sniff maintenance diet, Soest Germany) and under standard conditions. Three-week-old $Cyp2c70^{-/-}$ mice and their wild type littermates were terminated and their plasma and organs were collected for further analysis.

All animal experiments were performed in accordance with the Dutch law and approved by the Dutch Central Committee for Animal Experiments and the Animal Welfare Body of the University of Groningen.

### 2.2. Histology of BAT

The BAT samples were fixed in 4 % neutral buffered paraformaldehyde, embedded in paraffin, cut into 4-μm sections, and stained with either hematoxylin/eosin (H&E) or picrosirius red staining by standard procedures. Lipid droplets area was determined in H&E-stained sections by using ImageJ (National Institutes of Health, Bethesda, Maryland, USA), which automatically identified particles and quantified their area percentage.

### 2.3. Real-time quantitative reverse transcription-PCR

Total RNA was isolated from WAT and BAT using RNeasy Lipid Tissue Mini Kit (Qiagen), using TRIreagent (Sigma-Aldrich, St. Louis, MO, USA). cDNA was synthesized by reverse transcription using reverse transcriptase and random primers according to the manufacturer's protocol. mRNA expression levels were analyzed in MicroAmp optical 96-well plates using StepOne Real-Time PCR system (Applied Biosystems Europe, Nieuwerkerk aan den IJssel, The Netherlands). PCR results were normalized to 36B4 mRNA levels. Primers and probe sequences are listed in Table S1.

### 2.4. Affymetrix microarray analysis

Total RNA for microarray analysis was isolated using TRI reagent (Sigma-Aldrich, St. Louis, MO, USA). RNA was further purified using RNeasy MinElute micro columns (Qiagen, Venlo, Netherlands). RNA integrity was checked on an Agilent 2100 bioanalyzer (Agilent Technologies, Amsterdam, Netherlands) using 6000 Nano Chips according to the manufacturer's instructions. Five hundred nanograms of RNA were used for one cycle of cDNA synthesis (Affymetrix, Santa Clara, CA). Subsequently, samples were hybridized, washed and scanned on the Affymetrix Gene chip mouse arrays according to standard Affymetrix protocols. Quality control of microarray data, normalization and

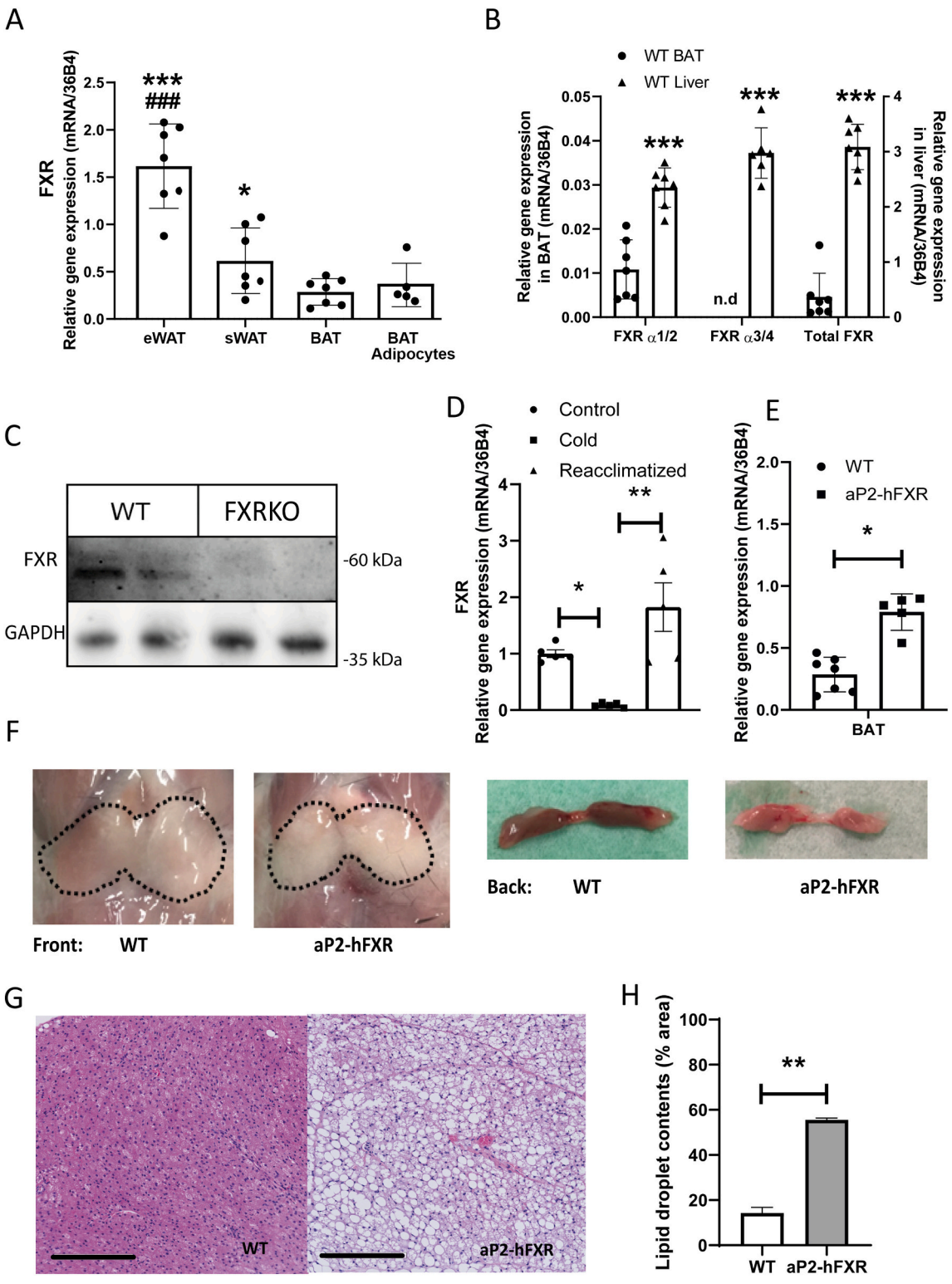


**Fig. 1.** Whitened BAT in aP2-hFXR mice. (A) Quantitative real-time PCR of total FXR expression in epididymal adipose tissue (eWAT), subcutaneous adipose tissue (sWAT) and brown adipose tissue (BAT) as well as isolated adipocytes from BAT, of chow-fed wild-type (wt) mice aged 12 weeks. (B) Quantitative real-time PCR of FXRα1/2, FXRα3/4 and total FXR expression in BAT and liver from wt mice. (C) Western blot analysis of FXR protein levels in BAT of chow-fed wt and total FXRKO mice. (D) Quantitative real-time PCR of FXR expression in BAT during cold exposure. (E) Quantitative real-time PCR of total FXR expression brown adipose tissue (BAT) of chow-fed wt and adipocyte-specific FXR overexpressing male mice (aP2-hFXR) aged 12 weeks. (F) BAT gross morphology from back and front sides of wt and aP2-hFXR mice, dash line circles the interscapular BAT. (G) Representative image of H&E staining of BAT morphology showing whitening of BAT in aP2-hFXR mice. Bar represents 200 μm. (H) Relative lipid droplets in BAT tissue sections. Statistical significance was determined using the Mann-Whitney test for BAT in wt and aP2-hFXR mice. All panels: N = 5–7/group, data are represented as mean ± SD, *p < 0.05, ** p< 0.01, *** < 0,001 when compared with BAT in panel A; $^{###}$p < 0.001 when compared with sWAT.

differential expression analysis were performed through the Management and Analysis Database for MicroArray experiments analysis pipeline (Wageningen, Netherlands). Expression levels of probe sets were calculated using Limma, a regular normalization strategy. Comparison was made between treated (aP2-hFXR mice) and untreated (wild-type mice) groups. A false discovery rate (FDR) <5 % was used as a threshold for significance of differential expression. Differentially expressed genes that had FDR adjusted p value <0.01 and the fold change at least 2 times higher or lower were used in R-3.31 to present volcano plot and top 100 differentiation genes were used for hierarchical clustering. Identification of overrepresented functional categories among all responsive genes and their grouping into functionally related clusters (Biological Processes, Cellular Components, Molecular Function and KEGG Pathway) was performed using the DAVID Functional Annotation Clustering tool [32]. Data reported are available in the GEO database (GSE37248) and in accordance with MIAME guidelines.

### 2.5. Western blotting

To quantify FXR, UCP1 and C/EBPβ proteins, Western blotting was performed. BAT lysates were prepared in RIPA lysis buffer (Tris-HCL pH = 8, NaCl 138 mM, NP40 1 %, KCL 2.7 mM, MgCl2 1 mM, Glycerol 5 %, EDTA 5 mM, $Na_3VO_4$ 1 mM, NaF 20 mM, DTT 1 mM and protease inhibitor) and protein concentrations were quantified using Pierce BCA protein assay kit (Thermo Fisher Scientific, Netherlands). Samples from isolated adipocytes were obtained by established procedures [33] Protein samples were subjected to SDS-PAGE (4–15 % gels) and transferred to nitrocellulose using Trans-Blot® Turbo™ transfer system (Bio-Rad). Membranes were blocked for 1 h at room temperature in PBS containing 0.1 % Tween and 2 % BSA and incubated overnight with primary antibodies at 4 °C. Antibodies used in this study are: anti-FXR (Sc1204 Santa Cruz, Dallas, USA), anti-UCP1 (Abcam, Cambridge, United Kingdom), anti-C/EBPβ (Abcam, Cambridge, United Kingdom), anti-Tom20 (Santa-Cruz), anti-Acc (Cell signalling technology, Danvers, USA), anti-FAS (Cell Signaling), Oxphos-cocktail (Abcam) and anti-GAPDH (Calbiochem, San Diego, USA). Proteins were detected by incubating the blot with horseradish peroxidase (HRP)-conjugated donkey anti-rabbit (Life science, NA934) or HRP-conjugated rabbit anti-mouse (Dako, p0260) IgG for 1 h at room temperature. Bands were visualized using Supersignal West Dura substrate (Thermo Fisher Scientific, Netherlands) and ChemiDoc (Bio-Rad).

### 2.6. Indirect calorimetry

Indirect calorimetry was used to study the energy metabolism of aP2-hFXR mice during cold exposure and β3-adrenergic receptor agonist treatment. Mice were placed in an open-circuit indirect calorimeter system 24 h prior to the start of the experiment with free access to water and food (TSE systems GmbH, Bad Homburg, Germany). Flow rates were measured and controlled with a mass flow controller and $O_2$ as well as $CO_2$ concentrations were measured in dried inlet and outlet air from each chamber. Infrared light-beam frames surrounding the home cage measured activity in the x and y direction. Data were analyzed using LabMaster software (TSE systems GmbH, Bad Homburg, Germany). Energy expenditure was calculated using the following equation: EE (kcal/h) = 3.941 × $VO_2$ (l/h) + 1.106 × $VCO_2$ (l/h).

### 2.7. Plasma metabolite measurements

Plasma glucose levels were measured by a Performa glucometer (Accu-Chek, Netherlands). Free fatty acids (FFA) were determined using a commercially available kit (DiaSys Diagnostic Systems, Holzheim, Germany). Bile acids in plasma were measured by ultra high-performance liquid chromatography tandem mass spectrometry [31].

### 2.8. Determination of mitochondrial DNA copy number

Mitochondrial DNA (mtDNA) copy number was determined according to van Zutphen et al. [34]. Specifically, total DNA was isolated from BAT using GenElute™ Mammalian Genomic DNA Miniprep Kit (Sigma-Aldrich, Zwijndrecht, Netherlands). The mtDNA copy number was assessed by determining the ratio of copy numbers of the mitochondrial genome-encoded ATP synthase subunit 6 (mt-Atp6) gene (mtDNA) relative to the single copy nuclear peroxisome proliferator activated receptor-γ coactivator-1α (Ppargc1α) gene (nuclear DNA). The primers were listed in Table S1. Real-time PCR was performed in MicroAmp optical 96-well plates using StepOne Real-Time PCR system (Applied Biosystems). The reaction volume of 15 μl contained 10 ng of genomic DNA, forward and reverse primers (0.25 μM each) and SYBR mastermix.

### 2.9. Statistical analysis

Data are presented as mean ± SD. Differences between two groups were tested by non-parametric Mann-Whitney *U* test, multiple groups by Kruskal-Wallis H-test followed by post-hoc Connover test using Graphpad Prism 8.00 software package (GraphPad Software, San Diego, CA, USA). For correlations, the Pearsons correlation coefficient was determined after testing for normal distribution with a Kolmogorov-Smirnov test. Unless otherwise noted, significance was indicated as *$p < 0.05$, **$p < 0.01$, ***$p < 0.001$.

## 3. Result

### 3.1. *Fxr* is expressed in murine BAT and is down-regulated upon cold exposure

To study the potential role of FXR in BAT, we assessed *Fxr* expression in murine BAT and WAT depots. In line with earlier data from our laboratory [35], *Fxr* expression in BAT from wild-type mice was considerably lower than in subcutaneous and epididymal WAT depots and ~99 % lower than in liver (Fig. 1A, B). Yet, *Fxr* expression was clearly detectable, exclusively representing the α1/2 isoforms (Fig. 1B). *Fxr* expression levels in isolated mature adipocytes were similar to BAT tissue (Fig. 1A). A distinct protein band with a molecular weight of 55 kDa could be detected in BAT from wild-type mice and was absent in BAT from $FXR^{-/-}$ mice (Fig. 1C). To determine whether *Fxr* expression is impacted by functional activation of BAT, wild-type mice were exposed to cold. These mice showed a marked but reversible decrease of *Fxr* expression in BAT compared to control mice that remained at ambient temperature (Fig. 1D).

### 3.2. Moderate overexpression of FXR in adipose tissues leads to whitening of BAT

As a decrease in endogenous *Fxr* expression in BAT upon activation by cold exposure was observed, we employed the aP2-driven overexpression model of the human α2 isoform, which is also expressed in BAT [12], to assess potential functions of FXR in BAT. Total *Fxr* mRNA expression level was significantly (2.5-fold) higher in BAT of the aP2-hFXR mice compared to wild-type controls (Fig. 1E). BAT from wild-type mice showed the characteristic brown colour due to the presence of abundant densely-packed, iron-rich mitochondria. However, interscapular BAT of aP2-hFXR mice showed a clearly lighter colour than that of control mice (Fig. 1F). H&E staining showed that BAT from aP2-hFXR mice was filled with large lipid droplets (Fig. 1G). Remarkably, this whitened BAT resembled WAT and quantification of the lipid droplet content showed a marked increase in droplet surface area in BAT of aP2-hFXR mice compared to controls (Fig. 1H). As gender differences exist in metabolic flexibility that includes adipose tissue function, BAT of female aP2-hFXR was also analyzed. Accumulation of lipid droplets was also

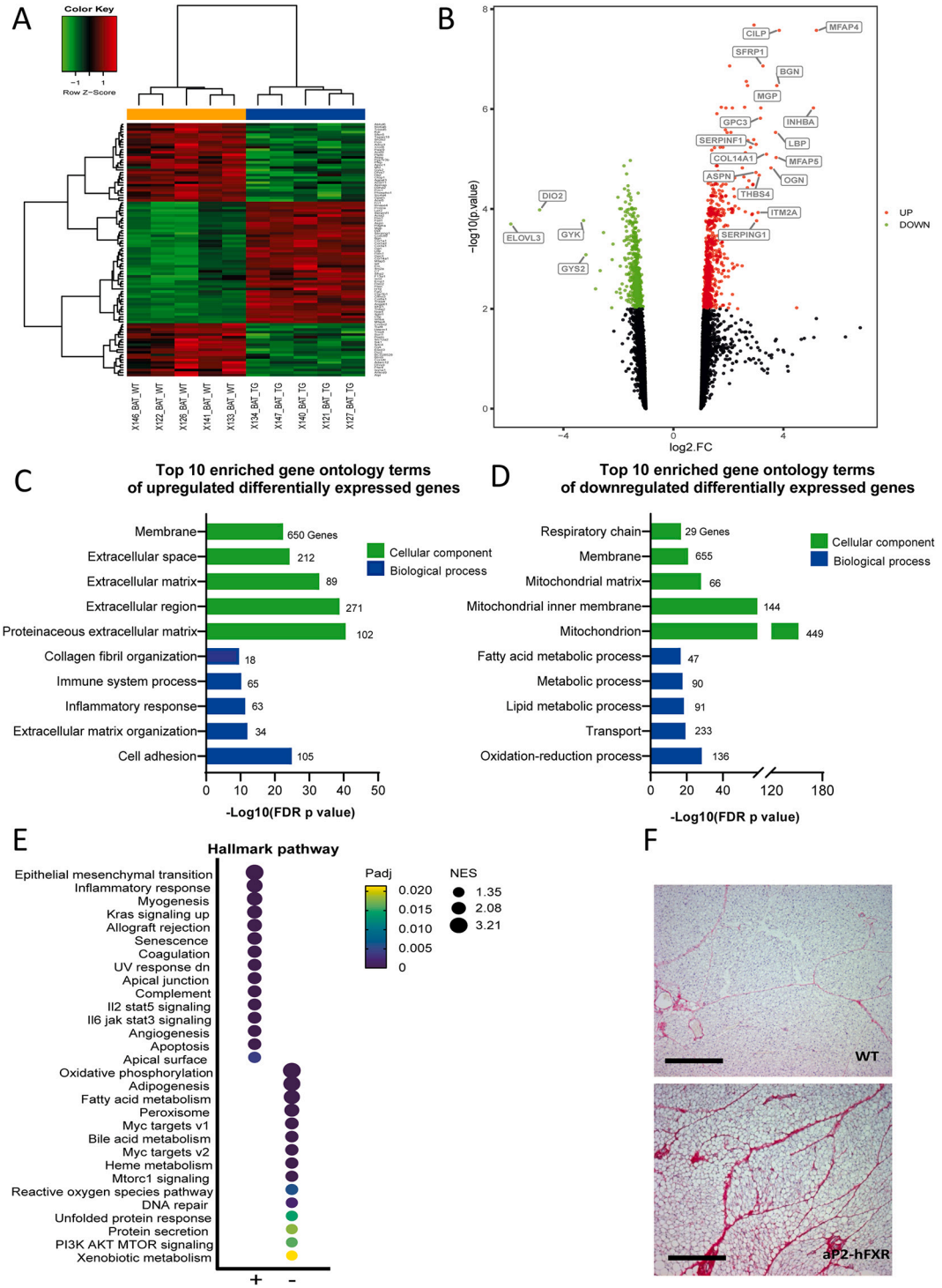


**Fig. 2.** BAT ECM remodelling in aP2-hFXR mice. (A) Heat map of top 100 mostly differentially expressed genes in brown adipose tissue (BAT) of chow-fed wild type (wt) and adipocyte-specific FXR overexpressing male mice (aP2-hFXR) aged 10 weeks from microarray analysis, N = 5/group, FDR $\leq$ 5 %, $|\log2FC| \geq 2$ and the differentiation genes were ranked by their fold change. (B) Volcano plots of BAT wt and aP2-hFXR mice. Red and green dots are significantly up-regulated and down-regulated genes between wt and aP2-hFXR mice, $|\log2FC| \geq 2$; black dots represent genes without significant changes. $|\log2FC|$ of labeled genes are above 3. (C and D) Top 15 enriched gene ontology terms of downregulated and upregulated differentially expressed genes. Gene ontology terms include cellular component and biological process. (E) Pathway analysis using hallmark gene set collection from MSigDB on genes differentially expressed in BAT from wt and aP2-hFXR mice. Normalized enrichment scores (NES) of each pathway are indicated by bubble sizes and their adjusted p-value (padj) is indicated by bubble colour. Positive enrichment (+) and negative enrichment (−). (F) Collagen characterization in BAT of chow-fed wt and aP2-hFXR mice aged 14 weeks by Picosirius red staining, N = 6–8/group, bar represents 200 μM. DIO2 = dodothyronine deiodinase 2; GYS2 = glycogen synthase 2; ELOVL3 = ELOVL fatty acid elongase 3; GYK = glycerol kinase; MFAP4 = microfibrillar-associated protein 4; CILP = cartilage intermediate-layer protein; SFRP1 = secreted frizzled-related protein 1; BGN = biglycan; MGP = matrix Gla protein; GPC3 = glypican 3; INHBA = inhibin, beta A; SERPINF1 = serpin peptidase inhibitor, clade F; LBP = lipopolysaccharide binding protein; MFAP5 = microfibrillar-associated protein 5; COL14A1 = collagen, type XIV, alpha 1; ASPN = aspirin; OGN = osteoglycin; THBS4 = thrombospondin 4; SERPING1 = serpin peptidase inhibitor, clade G (C1-inhibiting factor); ITM2A = Integral membrane protein 2A.

observed in BAT of female aP2-hFXR mice compared to controls (Supplementary Fig. 1).

### 3.3. FXR modulates adipogenesis and extracellular matrix remodelling of BAT

An Affymetrix microarray experiment was performed, comparing BAT from aP2-hFXR and control mice, to gain insight into biological processes involved in FXR-mediated BAT remodelling. A total of 2992 genes were differentially expressed in aP2-hFXR vs. wild-type BAT (FDR $\leq$ 5 %). Heatmap analysis showing the top 100 differentially expressed genes revealed a distinct clustering of aP2-hFXR mice compared to control mice (Fig. 2A). Among the 112 genes that showed >2-fold difference in expression, 13 were found to be down-regulated while 99 were up-regulated in BAT of aP2-hFXR mice (Fig. 2B).

Genes related to extracellular matrix, such as those encoding collagens I, IV, VI and XV, were apparent among the up-regulated genes (Fig. 2B). Indeed, functional enrichment analysis of the differentially expressed genes identified extracellular matrix, collagen fibril organization, extracellular matrix organization and immune and -inflammatory responses as most prominent cellular components and biological processes in BAT of aP2-hFXR mice compared to controls (Fig. 2C). At the other side of the spectrum, *Dio2* was identified as one of the most strongly down-regulated genes, as well as glycogen synthesis 2 (*Gys2*) and elongation of very long chain fatty acid 3 (*Elovl3*), the latter important for lipid recruitment in BAT (Fig. 2B) [36]. Functional annotation analysis showed that mitochondria, mitochondrial processes and lipid metabolism were among the most important down-regulated components and biological processes, respectively (Fig. 2D).

Hallmark pathway enrichment analysis showed BAT developmental processes to be affected: epithelial mesenchymal transition and myogenesis were identified as major up-regulated pathways, while adipogenesis was among the most down-regulated pathways (Fig. 2E). To confirm this unexpected finding, expression of muscle marker genes was quantified by qPCR analysis [37]. The expression levels of the early phase muscle differentiation marker myogenic factor 5 (*Myf5*), differentiation marker myosin-1 (*Myh1*) and myogenin (*Myog*) were indeed significantly increased in aP2-hFXR mice (Supplementary Fig. 2A). QPCR analysis of inflammatory marker gene expression levels confirmed the increased expression of monocyte attractant protein (*Mcp1*), interleukin 6β (*IL6 β*), cyclooxygenase 2 (*Cox2*) and intercellular adhesion molecule (*Icam*), but not of tumour necrosis factor α (*Tnfα*), in BAT of aP2-hFXR mice compared to controls (Supplementary Fig. 2B). We previously detected human *Fxr* expression in macrophages isolated from spleens of aP2-hFXR mice [12]. However, no effects on inflammation markers were observed in these macrophages [12]. Therefore, the observed changes in inflammation markers appear to be specific for BAT. Next to collagen-encoding genes, also other extracellular matrix (ECM) factors like elastin, biglycan and lumican, and ECM-modifying genes, such as cathepsins and metalloproteinases were up-regulated in aP2-hFXR mice. The accumulation of collagens was confirmed by picosirius-red staining, showing fibrosis in BAT of aP2-hFXR mice kept on chow diet (Fig. 2F) and significantly higher expression of collagens type I alpha 1 and alpha 2 (*Col1a1*, *Col1a2*) and tissue inhibitor of metalloproteinases 1 (*Timp1*) in BAT from aP2-hFXR mice (Supplementary Fig. 2C). Fibrosis has been reported to be associated with stem cell lineage fate, but also with cellular senescence in WAT and liver [38–40]. Pathway enrichment analysis indeed also showed cellular senescence genesets to be enriched in BAT of aP2-hFXR mice (Fig. 2D, Supplementary Fig. 2E, and Supplementary Table 2). Together, these results indicate compromised BAT development with strong extracellular matrix remodelling in the presence of moderately elevated *Fxr* expression.

### 3.4. Overexpression of hFXR results in decreased expression of thermogenesis genes

BAT is considered responsible for non-shivering thermogenesis [41]. The most well-described modulator of this process is UCP1, which redirects the proton-motive force in mitochondria leading to production of heat instead of ATP. To assess BAT function in aP2-hFXR mice, we first compared the expression levels of thermogenic genes in aP2-hFXR and control mice at room temperature. The aP2-hFXR mice showed a significantly lower expression of *Ucp1* mRNA (Fig. 3A) and UCP1 protein (Fig. 3B) in BAT. Expression of other thermogenesis marker genes, like *Dio2*, PR domain containing 16 (*Prdm16*), peroxisome proliferator-activated receptor gamma coactivator-1 alpha and beta (*Pgc1α* and *Pgc1β*), was also significantly decreased in aP2-hFXR mice (Fig. 3A). Furthermore, several genes related to mitochondrial oxidation, such as pyruvate dehydrogenase kinase 4 (*Pdk4*) and long chain acyl-CoA dehydrogenase (*Lcad*), were significantly decreased in aP2-hFXR mice. The transgenic mice showed decrease in mitochondrial DNA copy number (Fig. 3C) that was accompanied by decreased levels of the mitochondrial marker Tom20 as well as several markers for the oxidative phosphorylation complexes (Fig. 3D). Expression of BAT development marker genes like CCAAT/enhancer binding protein alpha and beta (*Cebpα*, *Cebpβ*) was also significant lower in aP2-hFXR mice (Fig. 3A) with a more pronounced decrease of the CEBP beta isoform liver-enriched inhibitory protein (LIP) compared to the liver activating protein (LAP) isoform in aP2-hFXR mice compared to wild-type mice (Fig. 3B). Interestingly, we found that expression of several fatty acid transporters was also significantly lower in aP2-hFXR mice (Fig. 3A). Although WAT lipolysis correlates strongly with plasma FFA levels [42], this decrease in BAT fatty acid transporters was also associated with increased plasma FFA in these animals (Fig. 3E). Besides fatty acid transport, protein levels of the major lipogenesis enzymes Acetyl-CoA carboxylase and Fatty acid synthase were also decreased in BAT of aP2-hFXR mice, indicating that lipogenesis is affected, a pathway that has been previously implicated in BAT involution (Fig. 3B) [43]. Phosphorylation of the protein kinase A-sensitive site on hormone sensitive lipase (Ser660) was similar to that in wildtype mice, indicating that β-adrenergic receptor signalling in BAT is unaltered in aP23-hFXR mice.

To exclude potential effects of FXR in other organs and tissues we also measured thermogenic marker genes in aP2-hFXR mice crossed onto the whole body $FXR^{-/-}$ background. These mice also clearly showed a whitened BAT phenotype when compared to $FXR^{-/-}$ controls (Supplementary Fig. 3A). A similar gene expression pattern as found in aP2-hFXR mice on the wild-type background was observed as well compared to the $FXR^{-/-}$ controls (Supplementary Fig. 3B).

To explore potential functional consequences of altered BAT architecture, a cold exposure experiment was performed. As observed previously, body weight was decreased in aP2-hFXR mice, yet food intake and physical activity during cold exposure were comparable (Supplementary Fig. 4A–C) Oxygen consumption by aP2-hFXR did not increase to the same extend as in control animals upon cold exposure (Fig. 3F, G). Responses to cold exposure were also examined at the gene expression level in BAT (Fig. 3H). The results show that the cold-associated induction in expression was less pronounced in aP2-hFXR compared to wild-type mice for *Prdm16*, *Cebpβ*, *Pgc1α*, *Dio2*, *Ucp1* and *Ucp3*. Collectively, these data identify FXR as a modulator of BAT activity.

To determine whether other tissues were also involved in the cold response, *Ucp1*, *Ucp2* and *Ucp3* expression was examined in different white fat depots, liver and muscle (Supplementary Fig. 4D–F). *Ucp1* was almost undetectable in liver, muscle and eWAT. Cold exposure seemed to induce *Ucp1* in sWAT, but to a much lower extend in aP2-hFXR mice. However, there was no significant difference in expression levels of *Ucp1*, *Ucp2* or *Ucp3* in either sWAT or eWAT between wild-type and aP2-hFXR mice at 4 °C compared to 21 °C. The 24-h of cold exposure did therefore not induce extensive browning of WAT yet (Supplementary Fig. 4D–F). Taken together, these results indicate that FXR modulates

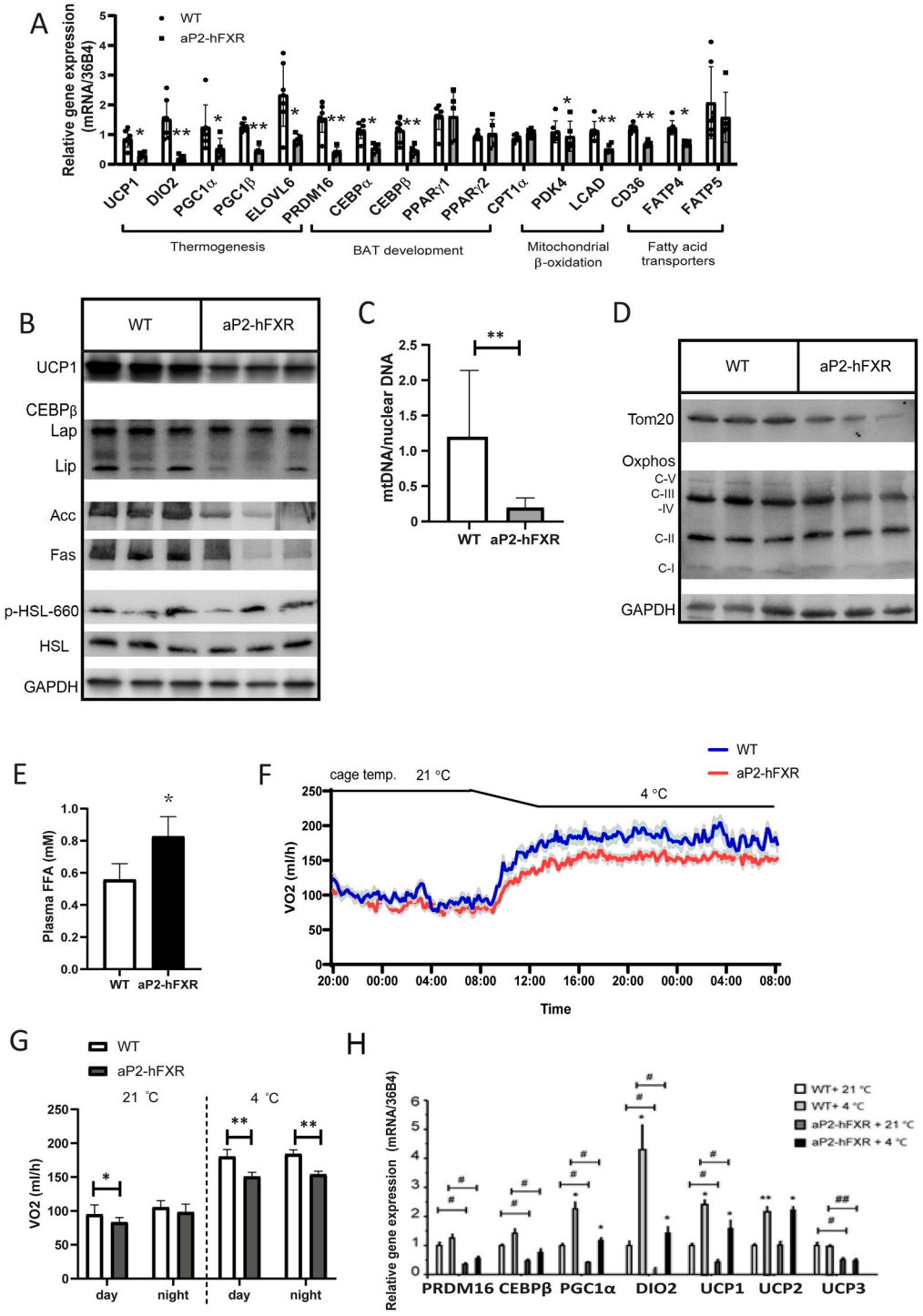


**Fig. 3.** Cold tolerance and expression of thermogenic genes. (A) Quantitative real-time PCR of thermogenic genes, BAT development, mitochondria β-oxidation and fatty acid transporters expression in brown adipose tissue (BAT) of wild-type (wt) and adipocyte-specific FXR overexpressing male mice (aP2-hFXR) aged 12 weeks, N = 5–7/group. (B) Western blot analysis of UCP1, CEBP, Acc, Fas, pHSL(Ser660) and HSL protein levels in BAT in chow-fed wt and aP2-hFXR mice (C) Mitochondrial DNA copy number in BAT of wt and aP2-hFXR mice, N = 10–12/group. (D) Western Blot analysis of Tom20 and Oxphos complexes (E) Plasma free fatty acids (FFA) in BAT in wt and aP2-hFXR mice, N = 5–7/group. (F) oxygen consumption, as measured in indirect calorimetry cages, of chow-fed wt and aP2-hFXR mice aged 14 weeks at 21 and 4 degrees, N = 7–8/group. Blue line with semi-transparent orange SD error bands represents wt mice; red line with semi-transparent grey SD error bands represents aP2-hFXR mice. Cage temp. represents the temperature of the cages. (G) Quantified oxygen consumption of wt and aP2-hFXR mice during day and night at 21 and 4 degrees. (H) Quantitative real-time PCR of thermogenic genes and mitochondria β-oxidation expression in BAT of chow-fed wt and aP2-hFXR mice aged 14 weeks at 21 and 4 degrees, N = 7–8/group. Panel A, C and E: Statistical significance was determined using the Mann-Whitney test in wt and aP2-hFXR mice. Data are represented as mean ± SD, *$p < 0.05$, **$p < 0.01$ when aP2-hFXR mice compared with wt mice. Panel H: Statistical significance was determined using Kruskal-Wallis H-test followed by post-hoc Conover pairwise comparisons. Data are represented as mean ± SEM, *$p < 0.05$, **$p < 0.01$ when mice at 4 °C compared with 21 °C; $^{\#}p < 0.05$, $^{\#\#}p < 0.01$ when aP2-hFXR mice compared with wt mice.

BAT architecture, yet BAT of transgenic mice appears to be able to respond to cold exposure, albeit not to the same extend as wild type mice.

### 3.5. The whitened BAT phenotype in aP2-hFXR mice can be rescued by β3- adrenergic receptor stimulation

We next questioned whether pharmacological adrenergic activation can rescue the whitened BAT phenotype in aP2-hFXR mice. For this purpose, we treated mice with the β3-adrenergic receptor agonist CL316243 for seven consecutive days. To confirm the acute metabolic response to the treatment, BAT substrates were analyzed. Plasma glucose levels decreased within 2 h after CL316243 injection in both wild-type and aP2-hFXR mice (Fig. 4A). Concomitant with the acute effects on plasma glucose, increased oxygen consumption was observed upon acute β3-adrenergic receptor activation in both genotypes. However, in contrast to control mice, the rise in oxygen consumption was less pronounced and only lasted for a few hours in aP2-hFXR mice (Fig. 4B), leading to a significantly smaller average increase in $VO_2$ during this peak during the 5 h after injection (Fig. 4C). In line with the lower oxygen consumption, aP2-hFXR mice also produced less $CO_2$ after CL316243 injection, leading to a lower calculated heat production (Fig. 4D, E).

To determine whether the treatment would eventually affect BAT morphology as well, in particular the whitened appearance, the treatment was prolonged in the same mice. After seven consecutive days of CL316243 treatment, there were no significant changes in body and liver weights compared to saline-treated controls (Supplementary Fig. 5A, B). In line with increased lipolysis, eWAT weight was reduced in CL316243-treated wild-type and aP2-hFXR mice compared to the non-treated controls (Supplementary Fig. 5C). Histological examination of BAT from wild-type and aP2-hFXR mice injected with saline or CL316243 revealed that lipid droplet prevalence in BAT from aP2-hFXR mice was strongly reduced after seven days of CL316243 treatment (Fig. 5A), indicating that the lipolytic β3-adrenergic receptor response is not affected by FXR overexpression. In wild-type mice, the expression of *Ucp1*, *Dio2* and *Prdm16* (but not of *Pgc1a*) was significantly increased after seven days of CL316243 treatment. However, in aP2-hFXR mice, only the increases in *Ucp1* and *Dio2* expression reached statistical significance but the levels of induction were lower than in treated wild-type mice (Fig. 5B). Among the genes related to mitochondrial β-oxidation, *Lcad* expression was significantly increased in wild-type mice, but not in aP2-hFXR mice, upon treatment. As bile acid-stimulated TGR5–cAMP–DIO2 signalling is important for thermogenesis [13] and as expression of *Dio2* was significantly decreased in aP2-hFXR mice, gene expression of *Tgr5* was determined. However, *Tgr5* expression did not significantly differ between aP2-hFXR mice and control mice with or without CL316243 treatment. As beige adipocytes in sWAT could also contribute to the physiological effects of β3 receptor activation and this treatment is known to stimulate browning of WAT, we also analyzed "BAT markers" in sWAT. In contrast to wild-type mice, which displayed a clear induction in *Ucp1*, *Dio2*, *Prdm16*, *Pgc1α* and *Elovl6* in sWAT upon treatment, this induction was strongly suppressed in aP2-hFXR mice (Fig. 5C). Collectively, these results propose a suppressive role for FXR in brown/beige adipocyte conversion and BAT function.

### 3.6. Altered thermogenic gene expression in BAT from suckling Cyp2c70-deficient mice with neonatal cholestasis

To explore whether exposure to elevated levels of FXR ligands, i.e., relatively hydrophobic bile acids, during early life would affect BAT development, the Cyp2c70$^{-/-}$ mouse model which displays a human-like bile acid profile and shows features of neonatal cholestasis [30,31] was studied. These mice display a similar body weight compared to wild type mice, yet have transient elevated plasma bile acids as well as transaminases. Suckling male and female Cyp2c70-deficient pups showed markedly elevated plasma bile acid levels upon weaning (Fig. 6A), including the natural FXR and TGR5 agonists DCA and LCA and was for approximately 75 % composed of the strongest natural FXR agonist CDCA, while lacking the FXR antagonistic muricholic acids (Fig. 6B). The Cyp2c70$^{-/-}$ pups showed decreased expression levels of thermogenic markers *Ucp1* and *Dio2* in BAT (Fig. 6C). At this age, mice rely on non-shivering thermogenesis to maintain body temperature and the model also does not present with hepatic collagen disposition and macrophage infiltration yet, as was previously observed in female mice upon early adulthood [30]. Expression levels of both bile acid sensors *Tgr5* and *Fxr* was similar in BAT of Cyp2c70$^{-/-}$ and wild-type controls (Fig. 6C). Histological examination of BAT revealed a higher degree of whitening in Cyp2c70$^{-/-}$ pups compared to wild-type pups (Fig. 6D). Quantification of lipid area confirmed that there was a significant increase in lipid mass in Cyp2c70$^{-/-}$ pups (Fig. 6E). In line with our observations in BAT of aP2-hFXR mice, markers of myogenic development, i.e., *Myf5* and *Myog*, were induced in BAT from Cyp2c70$^{-/-}$ pups (Fig. 6F), suggesting a role of bile acid signalling in BAT development. However, we did not observe obvious differences in the gene expression levels of fibrosis markers or inflammation markers in BAT from Cyp2c70$^{-/-}$ pups (Fig. 6F). The expression of *Ucp1* in BAT of mouse pups correlated with plasma bile acid levels (Fig. 6G), which was however not the case for *Dio2* (Fig. 6H), although expression of *Ucp1* and *Dio2* did still correlate with each other in BAT (Fig. 6I). Thus, it appears that mice with neonatal cholestasis show distinct features of derangements in BAT development that partly mirror the observed phenotype of BAT upon mild overexpression of adipose FXR. In mouse pups, plasma bile acid concentrations correlate with expression of the classical thermogenic marker *Ucp1* in BAT.

## 4. Discussion

Studies addressing the role of bile acids in the maintenance of energy homeostasis have mainly focused on TGR5 signalling in BAT, whereas FXR was considered to be absent in BAT [13,29]. However, in an earlier study [34] as well as in the current study, we were able to demonstrate the presence of *Fxr* mRNA, particularly encoding the α1/2 isoforms, and of FXR protein in BAT of wild-type mice. In addition, we found *Fxr* expression to be strongly and transiently suppressed upon BAT activation by cold exposure, suggestive for a functional role in adult mice. BAT of adult mice with stable, yet moderate overexpression of the human α2 isoform of FXR in adipose depots appeared to be whitened, with large, WAT-like lipid droplets. Furthermore, gene expression analysis revealed a pattern of decreased thermogenic gene expression, an increased myogenic gene expression profile as well as features of extracellular matrix remodelling and cellular senescence. Functional studies in aP2-hFXR mice indicated a blunted physiological response to cold exposure and β3-adrenergic receptor agonist treatment. Importantly, reduced expression of thermogenic genes was also observed in suckling Cyp2c70$^{-/-}$ mice with a human-like bile acid composition displaying neonatal cholestasis and *Ucp1* inversely correlated with plasma bile acid levels [30]. This indicates that bile acid signalling via FXR rather than via TGR5 may have a role in adequate development of BAT function in early life, a period in which plasma bile acid levels are also elevated in humans (physiological cholestasis) [44].

BAT has been reported to obtain a "whitened" appearance with obesity and aging, associated with reduced β-adrenergic signalling, mitochondrial dysfunction and loss of vascularity [45,46]. In our study, we found whitened BAT in adult chow-fed aP2-hFXR mice with increased collagen deposition and altered gene expression profiles of extracellular matrix proteins, which are of great importance for tissue integrity and functionality [47]. This results in a more fibrotic appearance of BAT in aP2-hFXR mice, which presumably results in a more rigid structure. Loss of ECM elasticity has been shown to be accompanied by a reduced capacity to interact with neighboring cells and to increase cellular senescence [48]. Cellular senescence marker genes, such as *p16*,

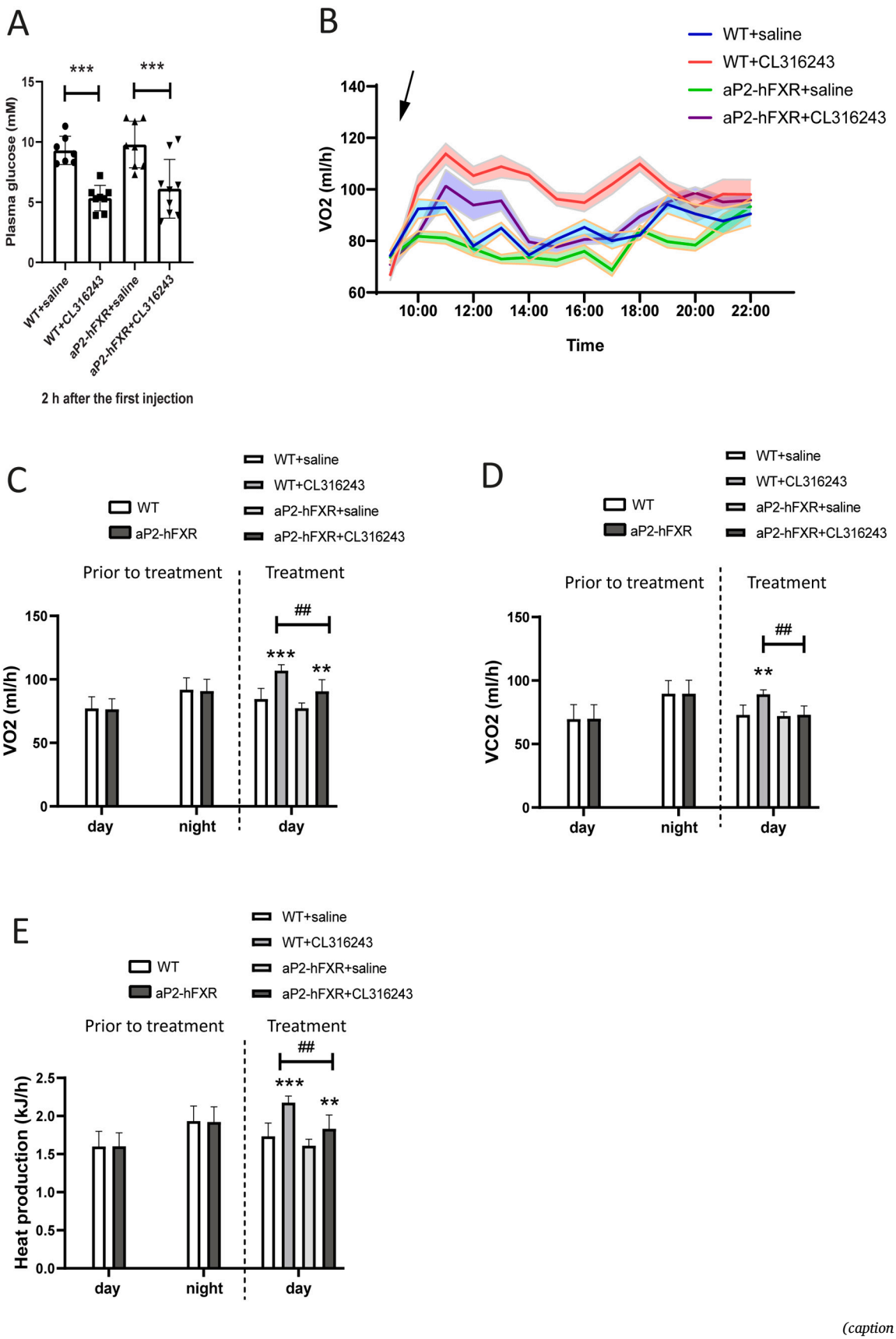


*(caption on next page)*

**Fig. 4.** Blunted BAT activation after acute CL316243 treatment in aP2-hFXR mice. (A) Plasma glucose levels (fed state) in wild type (wt) and adipocyte-specific FXR overexpressing male mice (aP2-hFXR) aged 16–20 weeks 2 h after the first injection of CL316243 or saline. (B) Oxygen consumption in indirect calorimetry cages before and after the first injection of saline or CL316243. Arrow represents the injection time point. Blue line with semi-transparent blue SD error bands represents wt mice treated with saline; red line with semi-transparent red SD error bands represents wt mice treated with CL316243; green line with semi-transparent green SD error bands represents aP2-hFXR mice treated with saline; purple line with semi-transparent purple SD error bands represents aP2-hFXR mice treated with CL316243. N = 5–7/group. (C) Quantified oxygen consumption, (D) carbon dioxide consumption and (E) heat production in wt and aP2-hFXR mice treated with and without CL316243, data before the dash line represents the results prior to treatment, 'day' represents the $VO_2$, $VCO_2$ or heat production per hour recorded by average 12 h during the day, 'night' represents the $VO_2$, $VCO_2$ or heat production per hour recorded by average 12 h during the night; data before the dash line represents the results after treatment, 'day' represents the $VO_2$, $VCO_2$ or heat production per hour recorded by average 5 h during the day from the moment of treatment representing the phase that an induction was observed in both treated groups. Statistical significance was determined using the Kruskal-Wallis test with post-hoc Conover analysis in wt and aP2-hFXR mice treated with CL316243 or saline. All panels: N = 7–9/group, data are represented as mean ± SD, $^{**}p < 0.01$, $^{***}p < 0.001$ when mice treated with CL316243 compared with mice treated with saline; $^{\#\#}p < 0.01$, when aP2-hFXR mice compared with wt mice.

*p53* and *Mapk*, as well as genes encoding for senescence-associated secretory phenotype factors, were clearly increased in BAT of aP2-hFXR mice. In WAT, senescence occurs predominantly in pre-adipocytes [49], however, whether this is also the case in BAT remains to be investigated. Previous studies also showed that microenvironment stiffness affects stem cell fate [38,50]. Together with the increased expression of muscle markers and decreased adipogenesis markers, these observations suggest that BAT structure and function in aP2-hFXR are compromised.

TGR5-mediated induction of *Dio2* has been proposed to link bile acids to thermal homeostasis via BAT activation [51]. Despite the elevated plasma bile acid levels observed previously in our model [12] and unaltered *Tgr5* expression, *Dio2* expression was significantly down-regulated in BAT from aP2-hFXR mice. Furthermore, expression of *Ucp1*, which plays an essential role in turning excess energy into heat and was shown to be up-regulated in mice lacking *Fxr* [14], as well as other BAT markers such as *Elovl3* showed decreased expression levels upon moderate *Fxr* overexpression [36]. In line with such a broad effect on most classical BAT marker genes as well as mitochondrial markers, we noticed that the PRDM16-C/EBPβ transcription regulatory complex, which regulates the differentiation and function of brown and beige fat, and its co-factors *Pgc1α* and *Pgc1β*, regulating long-chain fatty acid oxidation and mitochondrial functional capacity were all repressed by increased *Fxr* expression. Decreased levels of C/EBPβ, and predominantly of its dominant-negative inhibitor LIP isoform, were observed. A previous study showed that the LIP isoform was sufficient to rescue impaired adipogenesis caused by absence of the *Cebpβ* gene [52], indicating an important physiological function of the LIP isoform in adipocyte development. This provides a potential explanation for the overall suppressive activity of FXR in brown pre-adipocytes. AP2-driven overexpression of *GTF2IRD1*, a cofactor of the Prdm16 complex which was shown to regulate "the reciprocal relationship between fibrosis and brown/beige adipogenesis" [53], also resulted in a phenotype closely mirroring the aP2-hFXR model. Long-term treatment of mice with the FXR agonist GW4064 has been shown to decrease *Dio2*, *Pgc1a* and *Ucp1* expression in BAT and to induce its whitening [29]. The authors suggested that reduction of bile acid pool size may have caused these effects indirectly, yet our results indicate that direct action of the FXR agonist by FXR activation in BAT may contribute. Whether GW4064, and particularly hydrophobic bile acids, can enter brown adipocytes by active transport or through passive diffusion to activate FXR warrants further investigation.

Mice lacking *Cyp2c70* expression show a transient 10-fold elevation in plasma bile acids prior to weaning. These bile acids are strong endogenous ligands for both TGR5 and FXR. In marked contrast to expectations, a reduced expression of the TGR5 targets *Ucp1* and *Dio2* was observed, suggesting that the strong increase in CDCA and other ligands preferentially activated FXR leading to suppression of BAT markers. Indeed, an inverse correlation was identified between *Ucp1* and plasma bile acid levels, as well as a correlation between *Ucp1* and *Dio2*, although *Dio2* did not show a strong correlation with plasma bile acids. Possibly a simultaneous suppression of *Dio2* by FXR and stimulation by TGR5 obscures a clear-cut linear relation between these two parameters, whereas in the case of *Ucp1* the suppressive regulation by FXR apparently dominates the relation with bile acids. The suppression of thermogenic markers was also associated with whitening of BAT, indicating that a humanized bile acid pool with a relatively large amount of the FXR ligand CDCA causes accumulation of lipids in BAT of young mice. We can, however, not rule out that activation of FXR in other tissues, such as WAT, may modulate the accumulation of lipids in BAT.

Cariou et al. found that whole-body FXR deficiency in mice leads to severe cold intolerance with a rapid induction of torpor [14]. However, this effect might originate from hepatic FXR as part of the recently proposed BAT–liver–microbiome axis [54]. Whether prolonged cold exposure is also able to rescue the BAT whitening phenotype, as the chronic β3 adrenergic receptor agonist treatment did remains to be evaluated. As BAT size is limited, energy supplies need to come from elsewhere at some point during prolonged activation, especially from WAT [55]. The expression of fatty acid transporters in BAT was significantly lower in aP2-hFXR mice, suggesting that fuel utilization from external sources may be limited in sustaining long-term thermogenesis. In line, acute β3 receptor activation indeed led to both a suppressed as well as shorter induction of heat production, although this calculated heat production stemming from $O_2$ consumption and $CO_2$ production may not always equal actual heat production. Adipose triglyceride lipase (ATGL) deficiency also causes whitening of BAT in mice, yet ATGL in WAT is predominantly responsible for this phenotype [56]. Previous studies have shown that TGR5 agonism increases mitochondrial uncoupling in human brown adipocytes and administration of tauroocholic acid to high fat-diet fed mice and short term CDCA treatment of humans increases energy expenditure [13,57]. As the aP2-hFXR mouse model has elevated plasma bile acids with higher levels of cholate, taurocholate and muricholates yet lower levels of deoxycholate [12], there might be less TGR5 activation to trigger cAMP production. However, $FXR^{-/-}$ aP2-hFXR mice showed a similar whitened BAT phenotype as aP2-hFXR mice do. As these mice did not show elevated bile acid levels compared to their $FXR^{-/-}$ controls, while the whitened BAT was retained, an indirect route via liver-plasma bile acids activating -TGR5 in BAT, as was proposed previously for intestinal FXR-TGR5 interaction, is unlikely [58,59].

Whitening of BAT has been described in human obesity and as a consequence of ageing [60]. Increased inflammation was observed in the whitened BAT of aP2-hFXR mice, a condition that might contribute to impaired BAT functioning. Aggravation of the whitening process has also been described for models of leptin receptor-deficiency, absence of β-adrenergic signalling in brown adipocytes and by *Atgl* deficiency [46]. As these 3 models of BAT whitening were recently shown to cause inflammation rather than vice versa, this scenario is also likely to occur in our model [46]. Moreover, to exclude effects from aP2 promoter-induced off-target expression, we previously did not find an effect on inflammatory markers in WAT from obese mice or in isolated macrophages from our human *FXR* transgenic model and, importantly, FXR is known to suppress rather than to induce inflammation [12].

To summarize, FXR modulates BAT function and morphology at the level of tissue maintenance and development. FXR seems to act opposite and upstream to TGR5. This warrants caution with long-term use of FXR-

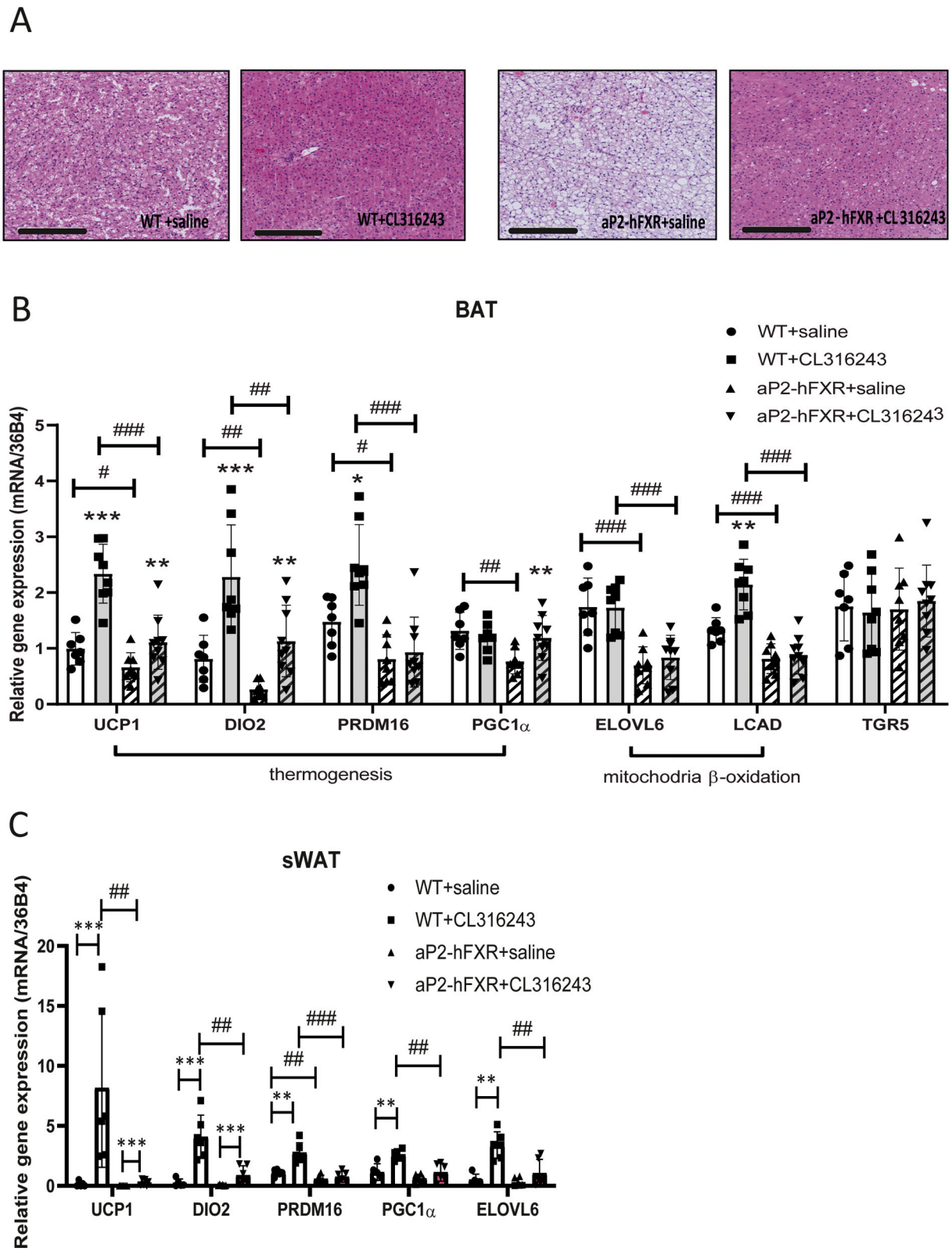


**Fig. 5.** Rescue of BAT whitening in aP2-hFXR mice by chronic CL316243. (A) Representative image of H&E staining of BAT morphology showing rescued phenotype of BAT in aP2-hFXR mice after 7 consecutive days of CL316243 or saline injection. Bar represents 200 μM. (B) Quantitative real-time PCR of thermogenic genes expression in BAT of chow-fed wt and aP2-hFXR mice after 7 consecutive days CL316243 or saline injection. (C) Quantitative real-time PCR of thermogenic genes expression in subcutaneous adipose tissue (sWAT) of chow-fed wt and aP2-hFXR mice after 7 consecutive days CL316243 or saline injection. Statistical significance was determined using the Kruskal-Wallis test with post-hoc Conover analysis in wt and aP2-hFXR mice treated with CL316243 or saline. Panel A, B, C, D: N = 7–9/group, data are represented as mean ± SD, $^{*}p < 0.05$, $^{**}p < 0.01$. $^{***}p < 0.001$ when mice treated with CL316243 compared with mice treated with saline; $^{\#}p < 0.05$, $^{\#\#}p < 0.01$. $^{\#\#\#}p < 0.001$ when aP2-hFXR mice compared with wt mice.

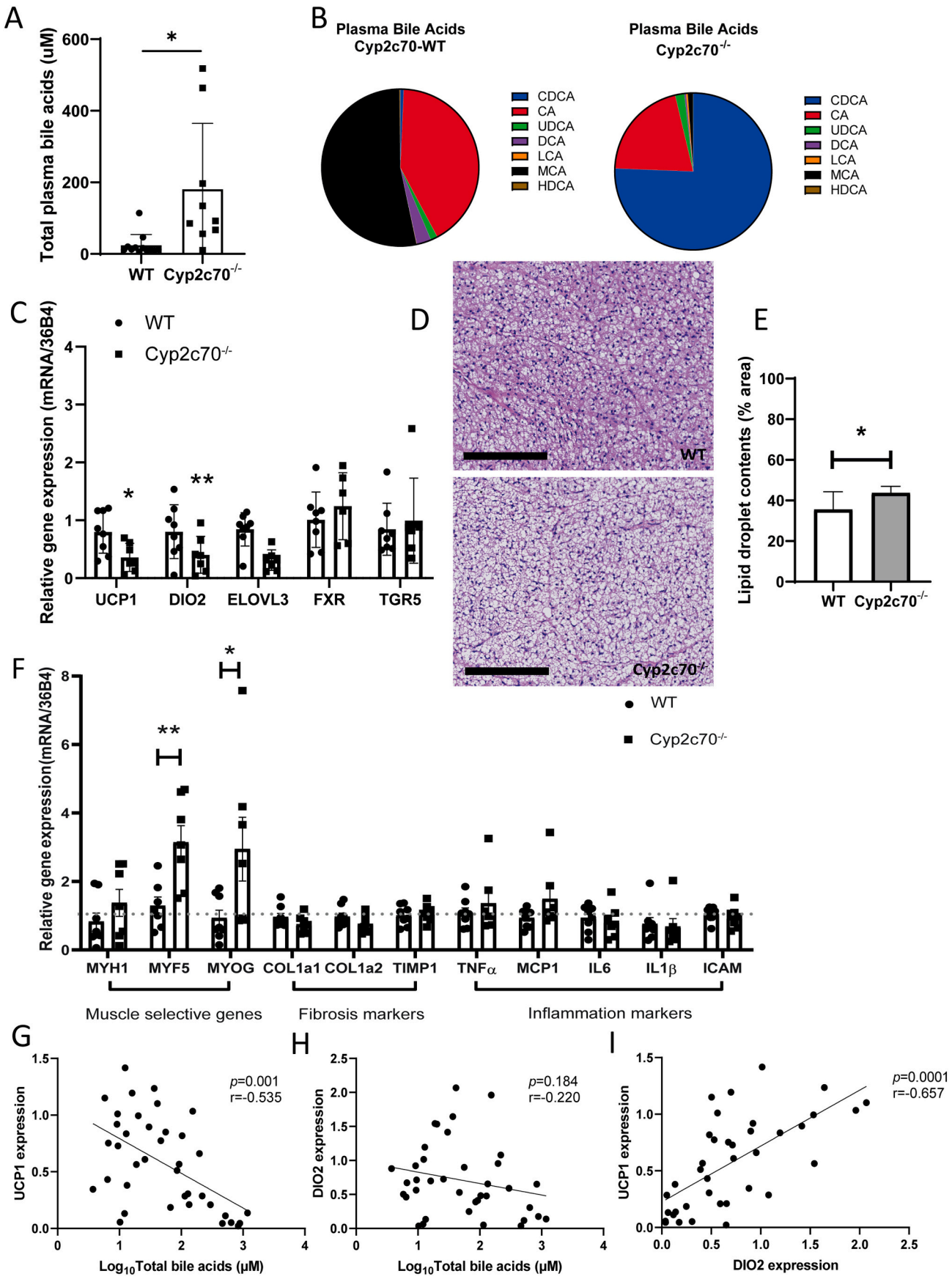


*(caption on next page)*

**Fig. 6.** Reduced BAT marker gene expression and increased whitening in young Cyp2c70-deficient mice with neonatal cholestasis. (A) Total plasma bile acid concentration and (B) plasma bile acid profile and in 3-week-old male and female wild-type (wt) and Cyp2c70$^{-/-}$ mice. (C) Quantitative real-time PCR of thermogenic gene expression as well as *Fxr* and *Tgr5* in BAT of chow-fed 3-week-old wt and Cyp2c70$^{-/-}$ mice. (D) Representative image of H&E staining of BAT morphology in 3-week-old wt and Cyp2c70$^{-/-}$ mice. Bar represents 200 μM. (E) Relative lipid droplet abundance in BAT tissue sections. (F) Quantitative real-time PCR of muscle selective genes, fibrosis markers and inflammation markers in BAT of 3-week-old wt and Cyp2c70$^{-/-}$ mice. (G) BAT *Ucp1* as well as (H) *Dio2* expression correlated with plasma bile acid levels of wild-type and Cyp2c70$^{-/-}$ mice. (I) *Ucp1* and *Dio2* correlation in BAT. Since there were no significant differences between male and female mice regarding to the data above, results for male and female cohorts were thus combined. Statistical significance was determined using the Mann-Whitney test in wt and Cyp2c70$^{-/-}$ mice and Pearson test for correlation. Data are represented as mean ± SD, *p < 0.05, **p < 0.01.

targeted therapeutics and identifies FXR as a modulator of browning and BAT function.

## CRediT authorship contribution statement

**J. Yang:** Methodology, Writing – original draft, Writing – review & editing. **H.D. de Vries:** Methodology. **A. Mayeuf-Louchart:** Methodology. **J.H. Stroeve:** Methodology. **V.W. Bloks:** Methodology. **M. Koehorst:** Methodology. **H. Duez:** Writing – review & editing. **B. Staels:** Writing – review & editing. **F. Kuipers:** Conceptualization, Writing – review & editing, Supervision. **T. van Zutphen:** Conceptualization, Writing – review & editing, Supervision.

## Declaration of competing interest

All authors have no conflict of interest.

## Data availability

Data reported are available in the GEO database (GSE37248).

## Acknowledgments

J.Y. is funded by China Scholarship Council (CSC).

## Appendix A. Supplementary data

Supplementary data to this article can be found online at https://doi.org/10.1016/j.bbalip.2022.159257.

## References

[1] J. Yang, A. Palmiotti, F. Kuipers, Emerging roles of bile acids in control of intestinal functions, Curr. Opin. Clin. Nutr. Metab. Care 24 (2021) 127–133, https://doi.org/10.1097/MCO.0000000000000709.
[2] F. Kuipers, V.W. Bloks, A.K. Groen, Beyond intestinal soap–bile acids in metabolic control, Nat. Rev. Endocrinol. 10 (2014) 488–498, https://doi.org/10.1038/nrendo.2014.60.
[3] G.A. Francis, E. Fayard, F. Picard, J. Auwerx, Nuclear receptors and the control of metabolism, Annu. Rev. Physiol. 65 (2003) 261–311, https://doi.org/10.1146/annurev.physiol.65.092101.142528.
[4] J.F. De Boer, V.W. Bloks, E. Verkade, M.R. Heiner-Fokkema, F. Kuipers, New insights in the multiple roles of bile acids and their signaling pathways in metabolic control, Curr. Opin. Lipidol. 29 (2018) 194–202, https://doi.org/10.1097/MOL.0000000000000508.
[5] S. Mudaliar, R.R. Henry, A.J. Sanyal, L. Morrow, H. Marschall, M. Kipnes, et al., Efficacy and safety of the farnesoid X receptor agonist obeticholic acid in patients with type 2 diabetes and nonalcoholic fatty liver disease, Gastroenterology 145 (2013) 574–582.e1, https://doi.org/10.1053/J.GASTRO.2013.05.042.
[6] B. Cariou, B. Staels, FXR: a promising target for the metabolic syndrome? Trends Pharmacol. Sci. 28 (2007) 236–243, https://doi.org/10.1016/J.TIPS.2007.03.002.
[7] B. Cariou, K. van Harmelen, D. Duran-Sandoval, T.H. van Dijk, A. Grefhorst, M. Abdelkarim, et al., The farnesoid X receptor modulates adiposity and peripheral insulin sensitivity in mice, J. Biol. Chem. 281 (2006) 11039–11049, https://doi.org/10.1074/jbc.M510258200.
[8] P. Lefebvre, B. Cariou, F. Lien, F. Kuipers, B. Staels, Role of bile acids and bile acid receptors in metabolic regulation, Physiol. Rev. 89 (2009) 147–191, https://doi.org/10.1152/physrev.00010.2008.
[9] G. Rizzo, M. Disante, A. Mencarelli, B. Renga, A. Gioiello, R. Pellicciari, et al., The farnesoid X receptor promotes adipocyte differentiation and regulates adipose cell function in vivo, Mol. Pharmacol. 70 (2006) 1164–1173, https://doi.org/10.1124/mol.106.023820.
[10] J. Prawitt, M. Abdelkarim, J.H.M. Stroeve, I. Popescu, H. Duez, V.R. Velagapudi, et al., Farnesoid X receptor deficiency improves glucose homeostasis in mouse models of obesity, Diabetes 60 (2011) 1861–1871, https://doi.org/10.2337/DB11-0030.
[11] M. Abdelkarim, S. Caron, C. Duhem, J. Prawitt, J. Dumont, A. Lucas, et al., The farnesoid X receptor regulates adipocyte differentiation and function by promoting peroxisome proliferator-activated receptor-γ and interfering with the Wnt/β-catenin pathways, J. Biol. Chem. 285 (2010) 36759–36767, https://doi.org/10.1074/jbc.M110.166231.
[12] T. Van Zutphen, J.H.M. Stroeve, J. Yang, V.W. Bloks, A. Jurdzinski, H. Roelofsen, et al., FXR overexpression alters adipose tissue architecture in mice and limits its storage capacity leading to metabolic derangements, J. Lipid Res. 60 (2019) 1547–1561, https://doi.org/10.1194/jlr.M094508.
[13] M. Watanabe, S.M. Houten, C. Mataki, M.A. Christoffolete, B.W. Kim, H. Sato, et al., Bile acids induce energy expenditure by promoting intracellular thyroid hormone activation, Nature 439 (2006) 484–489, https://doi.org/10.1038/nature04330.
[14] B. Cariou, E. Bouchaert, M. Abdelkarim, J. Dumont, S. Caron, J.-C. Fruchart, et al., FXR-deficiency confers increased susceptibility to torpor, FEBS Lett. 581 (2007) 5191–5198, https://doi.org/10.1016/j.febslet.2007.09.064.
[15] M.J.R. Dawkins, J.W. Scopes, Non-shivering thermogenesis and brown adipose tissue in the human new-born infant, Nature 206 (1965) 201–202, https://doi.org/10.1038/206201b0.
[16] A.L. Carey, B.A. Kingwell, Brown adipose tissue in humans: therapeutic potential to combat obesity, Pharmacol. Ther. 140 (2013) 26–33, https://doi.org/10.1016/j.pharmthera.2013.05.009.
[17] B.P. Leitner, S. Huang, R.J. Brychta, C.J. Duckworth, A.S. Baskin, S. McGehee, in: Mapping of Human Brown Adipose Tissue in Lean and Obese Young Men 114, 2017, pp. 8649–8654.
[18] A.M. Cypess, S. Lehman, G. Williams, I. Tal, D. Rodman, A.B. Goldfine, et al., Identification and importance of brown adipose tissue in adult humans, N. Engl. J. Med. 360 (2009) 1509–1517, https://doi.org/10.1056/NEJMoa0810780.
[19] V. Peirce, S. Carobbio, A. Vidal-Puig, The different shades of fat, Nature 510 (2014) 76–83, https://doi.org/10.1038/nature13477.
[20] A. Bartelt, O.T. Bruns, R. Reimer, H. Hohenberg, H. Ittrich, K. Peldschus, et al., Brown adipose tissue activity controls triglyceride clearance, Nat. Med. 17 (2011) 200–206, https://doi.org/10.1038/nm.2297.
[21] C.G. Lee, D.K. Rhee, B.O. Kim, S.H. Um, S. Pyo, Allicin induces beige-like adipocytes via KLF15 signal cascade, J. Nutr. Biochem. 64 (2019) 13–24, https://doi.org/10.1016/J.JNUTBIO.2018.09.014.
[22] T. Becher, S. Palanisamy, D.J. Kramer, M. Eljalby, S.J. Marx, A.G. Wibmer, et al., Brown adipose tissue is associated with cardiometabolic health, Nat. Med. 27 (2021) 58–65, https://doi.org/10.1038/s41591-020-1126-7.
[23] J. Heeren, L. Scheja, Brown adipose tissue and lipid metabolism, Curr. Opin. Lipidol. 29 (2018) 180–185, https://doi.org/10.1097/MOL.0000000000000504.
[24] A. Bartelt, J. Heeren, Adipose tissue browning and metabolic health, Nat. Rev. Endocrinol. 10 (2014) 24–36, https://doi.org/10.1038/nrendo.2013.204.
[25] A.J. Silvester, K.R. Aseer, J.W. Yun, Dietary polyphenols and their roles in fat browning, J. Nutr. Biochem. 64 (2019) 1–12, https://doi.org/10.1016/J.JNUTBIO.2018.09.028.
[26] J.M. Ntambi, K. Young-Cheul, Adipocyte differentiation and gene expression, J. Nutr. 130 (2000) 3122S–3126S, https://doi.org/10.1093/jn/130.12.3122S.
[27] S. Kim, J.W. Park, M.G. Lee, K.H. Nam, J.H. Park, H. Oh, et al., Reversine promotes browning of white adipocytes by suppressing miR-133a, J. Cell. Physiol. 234 (2019) 3800–3813, https://doi.org/10.1002/jcp.27148.
[28] S. Fang, J.M. Suh, S.M. Reilly, E. Yu, O. Osborn, D. Lackey, et al., Intestinal FXR agonism promotes adipose tissue browning and reduces obesity and insulin resistance, Nat. Med. 21 (2015) 159–165, https://doi.org/10.1038/nm.3760.
[29] M. Watanabe, Y. Horai, S.M. Houten, K. Morimoto, T. Sugizaki, E. Arita, et al., Lowering bile acid pool size with a synthetic farnesoid X receptor (FXR) agonist induces obesity and diabetes through reduced energy expenditure, J. Biol. Chem. 286 (2011) 26913–26920, https://doi.org/10.1074/jbc.M111.248203.
[30] J.F. de Boer, H.D. de Vries, A. Palmiotti, R. Li, M. Doestzada, J.A. Hoogerland, et al., Cholangiopathy and biliary fibrosis in cyp2c70-deficient mice are fully reversed by ursodeoxycholic acid, CMGH 11 (2021) 1045–1069, https://doi.org/10.1016/j.jcmgh.2020.12.004.
[31] J.F. De Boer, E. Verkade, N.L. Mulder, H.D. De Vries, N. Huijkman, M. Koehorst, et al., A human-like bile acid pool induced by deletion of hepatic Cyp2c70 modulates effects of FXR activation in mice, J. Lipid Res. 61 (2020) 291–305, https://doi.org/10.1194/jlr.RA119000243.
[32] G. Dennis, B.T. Sherman, D.A. Hosack, J. Yang, W. Gao, H.C. Lane, et al., DAVID: database for annotation, visualization, and integrated discovery, Genome Biol. 4 (2003), R60, https://doi.org/10.1186/gb-2003-4-5-p3.
[33] Y.D. Tchoukalova, S.B. Votruba, T. Tchkonia, N. Giorgadze, J.L. Kirkland, M. D. Jensen, Regional differences in cellular mechanisms of adipose tissue gain with overfeeding, Proc. Natl. Acad. Sci. U. S. A. 107 (2010) 18226–18231, https://doi.org/10.1073/pnas.1005259107.

[34] T. van Zutphen, J. Ciapaite, V.W. Bloks, C. Ackereley, A. Gerding, A. Jurdzinski, et al., Malnutrition-associated liver steatosis and ATP depletion is caused by peroxisomal and mitochondrial dysfunction, J. Hepatol. 65 (2016) 1198–1208, https://doi.org/10.1016/J.JHEP.2016.05.046.
[35] M. Boesjes, V.W. Bloks, J. Hageman, T. Bos, T.H. van Dijk, R. Havinga, et al., Hepatic farnesoid X-receptor isoforms α2 and α4 differentially modulate bile salt and lipoprotein metabolism in mice, PLoS One 9 (2014), e115028, https://doi.org/10.1371/journal.pone.0115028.
[36] R. Westerberg, J.E. Månsson, V. Golozoubova, I.G. Shabalina, E.C. Backlund, P. Tvrdik, et al., ELOVL3 is an important component for early onset of lipid recruitment in brown adipose tissue, J. Biol. Chem. 281 (2006) 4958–4968, https://doi.org/10.1074/jbc.M511588200.
[37] W. Wang, P. Seale, Control of brown and beige fat development, Nat. Rev. Mol. Cell Biol. 17 (2016) 691–702, https://doi.org/10.1038/nrm.2016.96.
[38] A.J. Engler, S. Sen, H.L. Sweeney, D.E. Discher, Matrix elasticity directs stem cell lineage specification, Cell 126 (2006) 677–689, https://doi.org/10.1016/j.cell.2006.06.044.
[39] E. Seki, D.A. Brenner, Recent advancement of molecular mechanisms of liver fibrosis, J. Hepatobiliary Pancreat. Sci. 22 (2015) 512–518, https://doi.org/10.1002/jhbp.245.
[40] K. Eckel-Mahan, A. Ribas Latre, M.G. Kolonin, Adipose stromal cell expansion and exhaustion: mechanisms and consequences, Cells 9 (2020) 863, https://doi.org/10.3390/cells9040863.
[41] R.N. Pradhan, M. Zachara, B. Deplancke, A systems perspective on brown adipogenesis and metabolic activation, Obes. Rev. 18 (2017) 65–81, https://doi.org/10.1111/obr.12512.
[42] V. Stich, M. Berlan, Physiological regulation of NEFA availability: lipolysis pathway, Proc. Nutr. Soc. 63 (2004) 369–374, https://doi.org/10.1079/PNS2004350.
[43] C. Schlein, A.W. Fischer, F. Sass, A. Worthmann, K. Tödter, M.Y. Jaeckstein, et al., Endogenous fatty acid synthesis drives Brown adipose tissue involution, Cell Rep. 34 (2021), 108624, https://doi.org/10.1016/j.celrep.2020.108624.
[44] W. Balistreri, F. Suchy, M. Farrell, J. Heubi, Pathologic versus physiologic cholestasis: elevated serum concentration of a secondary bile acid in the presence of hepatobiliary disease, J. Pediatr. 98 (1981) 399–402, https://doi.org/10.1016/S0022-3476(81)80702-0.
[45] I. Shimizu, K. Walsh, The whitening of brown fat and its implications for weight management in obesity, Curr. Obes. Rep. 4 (2015) 224–229, https://doi.org/10.1007/s13679-015-0157-8.
[46] P. Kotzbeck, A. Giordano, E. Mondini, I. Murano, I. Severi, W. Venema, et al., Brown adipose tissue whitening leads to brown adipocyte death and adipose tissue inflammation, J. Lipid Res. 59 (2018) 784–794, https://doi.org/10.1194/jlr.M079665.
[47] M.A. Gonzalez Porras, K. Stojkova, M.K. Vaicik, A. Pelowe, A. Goddi, A. Carmona, et al., Integrins and extracellular matrix proteins modulate adipocyte thermogenic capacity, Sci. Rep. 11 (2021) 5442, https://doi.org/10.1038/s41598-021-84828-z.
[48] A. Kurtz, S.J. Oh, Age related changes of the extracellular matrix and stem cell maintenance, Prev. Med. 54 (2012) S50–S56, https://doi.org/10.1016/j.ypmed.2012.01.003.
[49] T. Tchkonia, D.E. Morbeck, T. Von Zglinicki, J. Van Deursen, J. Lustgarten, H. Scrable, et al., Fat tissue, aging, and cellular senescence, Aging Cell 9 (2010) 667–684, https://doi.org/10.1111/j.1474-9726.2010.00608.x.
[50] K.M. Tharp, M.S. Kang, G.A. Timblin, J. Dempersmier, G.E. Dempsey, P.J. H. Zushin, et al., Actomyosin-mediated tension orchestrates uncoupled respiration in adipose tissues, Cell Metab. 27 (2018) 602–615, https://doi.org/10.1016/j.cmet.2018.02.005, e4.
[51] L.A. de Jesus, S.D. Carvalho, M.O. Ribeiro, M. Schneider, S.-W. Kim, J.W. Harney, et al., The type 2 iodothyronine deiodinase is essential for adaptive thermogenesis in brown adipose tissue, J. Clin. Invest. 108 (2001) 1379–1385, https://doi.org/10.1172/JCI13803.
[52] V. Bégay, C. Baumeier, K. Zimmermann, A. Heuser, A. Leutz, The C/EBPβ LIP isoform rescues loss of C/EBPβ function in the mouse, Sci. Rep. 8 (2018) 8417, https://doi.org/10.1038/s41598-018-26579-y.
[53] Y. Hasegawa, K. Ikeda, Y. Chen, D.L. Alba, D. Stifler, K. Shinoda, et al., Repression of adipose tissue fibrosis through a PRDM16-GTF2IRD1 complex improves systemic glucose homeostasis, Cell Metab. 27 (2018) 180–194, https://doi.org/10.1016/j.cmet.2017.12.005, e6.
[54] A. Worthmann, C. John, M.C. Rühlemann, M. Baguhl, F.-A. Heinsen, N. Schaltenberg, et al., Cold-induced conversion of cholesterol to bile acids in mice shapes the gut microbiome and promotes adaptive thermogenesis, Nat. Med. 23 (2017) 839–849, https://doi.org/10.1038/nm.4357.
[55] J. Nedergaard, T. Bengtsson, B. Cannon, New powers of brown fat: fighting the metabolic syndrome, Cell Metab. 13 (2011) 238–240, https://doi.org/10.1016/j.cmet.2011.02.009.
[56] R. Schreiber, C. Diwoky, G. Schoiswohl, U. Feiler, N. Wongsiriroj, M. Abdellatif, et al., Cold-induced thermogenesis depends on ATGL-mediated lipolysis in cardiac muscle, but not brown adipose tissue, Cell Metab. 26 (2017) 753–763, https://doi.org/10.1016/j.cmet.2017.09.004, e7.
[57] E.P.M. Broeders, E.B.M. Nascimento, B. Havekes, B. Brans, K.H.M. Roumans, A. Tailleux, et al., The bile acid chenodeoxycholic acid increases human brown adipose tissue activity, Cell Metab. 22 (2015) 418–426, https://doi.org/10.1016/j.cmet.2015.07.002.
[58] P. Pathak, H. Liu, S. Boehme, C. Xie, K.W. Krausz, F. Gonzalez, J.Y.L. Chiang, Farnesoid X receptor induces Takeda G-protein receptor 5 cross-talk to regulate bile acid synthesis and hepatic metabolism, J. Biol. Chem. 292 (2017) 11055–11069, https://doi.org/10.1074/jbc.M117.784322.
[59] P. Pathak, C. Xie, R.G. Nichols, J.M. Ferrell, S. Boehme, K.W. Krausz, et al., Intestine farnesoid X receptor agonist and the gut microbiota activate G-protein bile acid receptor-1 signaling to improve metabolism, Hepatology 68 (2018) 1574–1588, https://doi.org/10.1002/hep.29857.
[60] E. Zoico, S. Rubele, A. De Caro, N. Nori, G. Mazzali, F. Fantin, et al., Brown and beige adipose tissue and aging, Front. Endocrinol. 10 (2019) 368, https://doi.org/10.3389/fendo.2019.00368.